NeuroImage 49 (2010) 433–441

Contents lists available at ScienceDirect

NeuroImage

journal homepage: www.elsevier.com/locate/ynimg

Simplified parametric methods for [^{18}F]FDDNP studies

Maqsood Yaqub [a,*], Nelleke Tolboom [b], Bart N.M. van Berckel [a], Philip Scheltens [b], Adriaan A. Lammertsma [a], Ronald Boellaard [a]

[a] Department of Nuclear Medicine & PET Research, VU University Medical Centre, PO Box 7057, 1007 MB Amsterdam, The Netherlands
[b] Department of Neurology & Alzheimer Centre, VU University Medical Centre, PO Box 7057, 1007 MB Amsterdam, The Netherlands

ARTICLE INFO

Article history:
Received 30 March 2009
Revised 25 June 2009
Accepted 14 July 2009
Available online 28 July 2009

Keywords:
[^{18}F]FDDNP
Parametric methods
PET
Kinetic modelling
Reference tissue models

ABSTRACT

The purpose of the present study was to evaluate the performance of various parametric methods for quantification of [^{18}F]FDDNP studies. All parametric methods tested were based on the use of a reference tissue and they were compared with the simplified reference tissue model (SRTM), as previously it has been shown that SRTM is the method of choice for analysing [^{18}F]FDDNP studies, even when an arterial plasma input function is available. The following parametric methods were evaluated: receptor parametric mapping (basis function implementation of SRTM; with and without fixing the reference tissue efflux rate constant k'_2), reference Logan and several multi-linear reference tissue methods (again with and without fixing k'_2). Simulations were used to assess the effects of variation in relative flow (R_1), fractional blood volume (V_b) and binding potential (BP_{ND}) on precision and accuracy of estimated BP_{ND}. For clinical data, best performance was obtained using receptor parametric mapping (RPM2) and one of the multi-linear reference tissue models (MRTM2), with k'_2 being fixed in both methods. These models showed good correlation with SRTM, their BP_{ND} results were less affected by noise and images showed good contrast. Furthermore, in simulations, RPM2 and MRTM2 provided the most accurate and precise BP_{ND} estimates. RPM2 and MRTM2 are the methods of choice for parametric analysis of [^{18}F]FDDNP studies.

Introduction

[^{18}F]FDDNP is a ligand, that has been developed for imaging amyloid plaques and neurofibrillary tangles in the human brain *in vivo* using PET (Barrio et al., 1999). These plaques and tangles are present in the brain of patients with Alzheimer's disease (AD; Braak and Braak, 1997).

To date, use of parametric methods for analysing [^{18}F]FDDNP data has been limited to residence time within a cerebral region relative to that in pons (Shoghi-Jadid et al., 2002), standardized uptake value (SUV) and distribution volume ratio (*DVR*; Kepe et al., 2004) using Logan analysis with cerebellum as reference region (Logan et al., 1996). Recent studies, using reference Logan analysis, have reported increased levels of [^{18}F]FDDNP uptake (i.e. *DVR*) in neocortical regions of AD patients compared with both patient's own cerebellum (Kepe et al., 2004) and corresponding neocortical regions in healthy controls (Small et al., 2006).

Although, reference Logan analysis is an accepted parametric method, there are alternative parametric approaches, such as the use of basis functions (Gunn et al., 1997) and multi-linear analyses (Ichise et al., 2003). In addition, the impact of noise may be reduced by imposing additional parameter constraints (Wu and Carson, 2002). Furthermore, for the related tracer [^{11}C]PIB, it was shown (Zhou et al., 2007) that improvements in quantification could be achieved by coupling of parameters in the simplified reference tissue model (SRTM; Lammertsma and Hume, 1996). A study (Yaqub et al., 2008), evaluating different reference tissue based parametric methods in order to optimise quantification of [^{11}C]PIB studies, confirmed these improvements and showed several methods outperforming reference Logan.

In a recent validation study (Yaqub et al., 2009) using plasma input data, it was shown that SRTM is the method of choice for quantifying human [^{18}F]FDDNP data, providing more reproducible results than conventional plasma input methods. In addition, it was shown that, in contrast to other methods, SRTM gave a relatively constant bias in the presence of labelled [^{18}F]FDDNP metabolites. These metabolites are a concern as several studies have shown that they may enter the brain (Lubberink et al., 2007; Luurtsema et al., 2008).

The purpose of the present study was to investigate the accuracy and precision of various parametric methods for quantifying [^{18}F]FDDNP studies. These parametric methods would allow for the generation of fully 3D images of binding potential (BP_{ND}). A parametric method should be computationally fast and robust with respect to noise, which can be high at a voxel level. Based on the fact that SRTM was the method of choice at a region of interest (ROI) level (Yaqub et al., 2009), all parametric methods tested were reference tissue based and they were compared with SRTM. Methods included different approaches for reducing noise induced bias, such as the use of basis functions, multi-linear analyses and fixing the reference tissue efflux rate constant (k'_2). Performance of these parametric methods

* Corresponding author. Fax: +31 20 4443090.
E-mail address: Maqsood.Yaqub@VUmc.nl (M. Yaqub).

1053-8119/$ – see front matter © 2009 Elsevier Inc. All rights reserved.
doi:10.1016/j.neuroimage.2009.07.046

was evaluated using data from healthy controls, subjects with minimal cognitive impairment (MCI; Petersen et al., 2001) and AD patients. In addition, simulations were performed based on clinically relevant kinetic parameters. In these simulations, effects of blood volume, blood flow and noise on accuracy and precision of derived BP_{ND} values were studied.

Methods

Scanning protocol

Clinical data were derived from ongoing patient studies, approved by the Medical Ethics Review Committee of VU University Medical Centre, and consisted of 12 subjects (6 healthy controls, 3 MCI, and 3 AD) with an age ranging from 57 to 72 years (average 65 ± 5). Each subject gave written informed consent prior to inclusion in the study protocol. Clinical results are beyond the scope of the present study and will be reported elsewhere.

As part of the study protocol, each subject first underwent a T1-weighted MRI scan using a 1.5 T SONATA scanner (Siemens Medical Solutions, Erlangen, Germany). This MRI scan was performed to exclude anatomical abnormalities and for co-registration and segmentation purposes.

PET studies were performed using an ECAT EXACT HR+ scanner (CTI/Siemens, Knoxville, USA). The characteristics of this scanner have been described previously (Adam et al., 1997; Brix et al., 1997). For each study, first a 10 min transmission scan in 2D acquisition mode was performed, which was used to correct the subsequent emission scan for tissue attenuation. Next, a dynamic emission scan in 3D acquisition mode was performed following bolus injection of 168 ± 8 MBq [^{18}F]FDDNP. This scan consisted of 23 frames (1 × 15, 3 × 5, 3 × 10, 2 × 30, 3 × 60, 2 × 150, 2 × 300, 7 × 600 s) with a total scan duration of 90 min. Frames were reconstructed using FORE + 2D filtered back projection (Defrise et al., 1997) and a Hanning filter with a cut-off of 0.5 times the Nyquist frequency. Reconstructions included all usual corrections, such as normalization, and decay, dead time, attenuation, randoms and scatter (Watson, 2000) corrections.

Image analysis

The de-sculled T1-weighted MRI scans (Smith, 2002) were co-registered (Maes et al., 1997; West et al., 1997) with a summed PET image (frames 3–12: 25 s–5 min post injection). This summed image resembled a flow image, thereby maximizing cortical information. ROI were defined using an MR-based template (Svarer et al., 2005). For the purpose of the present study, grey matter ROI from 18 (cerebellum, orbital frontal cortex, medial inferior frontal cortex, anterior cingulate cortex, thalamus, insula, caudate, putamen, superior temporal cortex, parietal cortex, medial inferior temporal cortex, superior frontal cortex, occipital cortex, sensory motor cortex, posterior cingulate cortex, enthorinal cortex, hippocampus), all averaged over left and right hemispheres, were analysed.

Kinetic analysis

Clinical data were analysed at a pixel-by-pixel level using reference parametric mapping without and with fixing the reference tissue efflux rate constant k'_2 (RPM1 and RPM2; Gunn et al., 1997; Wu and Carson, 2002), reference Logan (Logan et al., 1996) and several multilinear reference tissue models (MRTMo, MRTM, MRTM2, MRTM3 and MRTM4; Ichise et al., 2003). For all these reference tissue based parametric methods cerebellum grey matter was used as reference tissue, as it is known to have low levels of amyloid plaques and neurofibrillary tangles (Braak and Braak, 1997; Joachim et al., 1989).

A detailed description of the methods, together with the settings used, can be found in Appendix A. In short, RPM1 and RPM2 are basis function implementations of SRTM. Reference Logan is a reference tissue adaptation of the (linear) Logan plot (Logan et al., 1990). MRTMo to MRTM4 are all variations of the reference Logan model, but with somewhat different assumptions, ordering of terms and use of multi-linear least squares. RPM1, reference Logan, MRTMo and MRTM are all fitted in a single run, whereas, RPM2, MRTM2, MRTM3 (MRTMo in second run) and MRTM4 (MRTM in second run) are fitted using two consecutive runs. After an initial run using a separate method (RPM1, MRTM, MRTMo and MRTMo for RPM2, MRTM2, MRTM3 and MRTM4, respectively), the median efflux rate constant k'_2 of the reference tissue is fixed in the second run to reduce the number of fit parameters. The pharmacokinetic parameter of interest estimated with all these methods is the binding potential BP_{ND}. For reference Logan BP_{ND} was estimated using DVR-1.

For comparison, ROI time activity curves (TAC) data were also analysed using SRTM. Parametric methods were evaluated by calculating average BP_{ND} values over these anatomical ROI and comparing them with BP_{ND} obtained with SRTM ($=BP_{ND}^{SRTM}$) using linear regression analysis and Bland–Altman plots (Bland and Altman, 1986).

Simulations

Clinical studies were analysed first to obtain estimates of the kinetic parameters. Based on these clinical results, simulated TAC were generated using a typical [^{18}F]FDDNP plasma input curve (Yaqub et al., 2009) in combination with a standard reversible two tissue compartment model (2T4k). In the simulations, variations in blood flow, blood volume and BP_{ND} were investigated for different noise levels.

Default parameters used for reference ($R1$) and target ($T1$) regions are listed in Table 1. First, only default parameters for reference tissue ($R1$) were used and parameters for target tissue BP_{ND} ($T1$–$T5$), fractional blood volume (V_b: $T1$, $T6$, $T7$) and delivery (K_1: $T1$, $T8$–$T11$), respectively, were varied. Next, to assess global changes in fractional blood volume and delivery, corresponding reference tissue TAC parameters were also varied ($R1$–$R7$). In these simulations each parameter was varied to the same degree in both target and reference regions. For each run 400 TAC were generated and each run was repeated at different noise levels ranging from 0 to 27% COV (coefficient of variation) in increments of 3%. This range was chosen

Table 1
Kinetic parameters used to generate reference (R) and target tissue (T) time activity curves (TAC).

TAC	K_1	BP_{ND}^{2T4k}	V_b	V_T	BP_{ND}^{2T4ki}
$R1$	0.35	1.63	0.050	8.7	–
$R2$	0.35	1.63	0.025	8.7	–
$R3$	0.35	1.63	0.075	8.7	–
$R4$	0.21	1.63	0.050	8.7	–
$R5$	0.28	1.63	0.050	8.7	–
$R6$	0.43	1.63	0.050	8.7	–
$R7$	0.50	1.63	0.050	8.7	–
$T1$	0.35	2.0	0.050	9.9	0.14
$T2$	0.35	1.7	0.050	8.9	0.03
$T3$	0.35	2.3	0.050	11	0.25
$T4$	0.35	2.6	0.050	12	0.37
$T5$	0.35	2.9	0.050	13	0.48
$T6$	0.35	2.0	0.025	9.9	0.14
$T7$	0.35	2.0	0.075	9.9	0.14
$T8$	0.21	2.0	0.050	9.9	0.14
$T9$	0.28	2.0	0.050	9.9	0.14
$T10$	0.43	2.0	0.050	9.9	0.14
$T11$	0.50	2.0	0.050	9.9	0.14

K_1 (ml cm^{-3} min^{-1}) is a rate constant, V_b fractional blood volume, V_T volume of distribution, and BP_{ND}^{2T4k} or BP_{ND}^{2T4ki} are binding potentials estimated using the two tissue reversible model and either direct (2T4k) and indirect (2T4k^i) approaches, respectively. In the indirect approach the volume of distribution ratios are used to estimate binding potential. During all simulations k_4 (0.032 min^{-1}) and K_1 / k_2 (3.3) were kept constant. Note that k_3 values used can be derived from $k_3 = BP_{ND}^{2T4k} \cdot k_4$.

to cover the entire range of clinically observed noise levels of ~5% (ROI averages) to ~15% (voxel values). Yet some higher noise levels were also included to be sure that the full clinical range was covered. Noise simulations were based on total scanner true counts, frame lengths and decay correction factors (Yaqub et al., 2006).

Simulated data were analysed using all parametric methods listed above. In addition, for comparison, corresponding noise free TAC were analysed using SRTM. For all parametric methods, bias (%) in derived BP_{ND} was assessed using $100*(BP^{x}_{ND} - BP^{SRTM}_{ND}) / BP^{SRTM}_{ND}$, where BP^{x}_{ND} is the apparent BP_{ND} from the parametric method.

Results

Human studies

Comparison with SRTM

Typical TAC of [^{18}F]FDDNP in cerebellum and a frontal ROI are shown in Fig. 1. Table 2 lists correlation coefficients obtained from linear regression analyses of the various parametric methods against BP^{SRTM}_{ND}. In general, all parametric methods showed high correlation with SRTM (R^2>0.96). The differences between the slopes were assessed using analysis of variance (ANOVA) with post-hoc Bonferroni test. The slope of MRTM3 versus those of all other methods, except MRTM and MRTM2, were significantly different at $p=0.05$ level. The slope of MRTM2 is showing the smallest difference (−0.0159) and that of MRTM the largest difference (−0.1613) with MRTM3. However, although MRTM showed the largest difference with MRTM3 it was not significantly different due to the large variability of the MRTM data. Detailed analysis of these correlations was furthermore performed using scatter (Fig. 2) and Bland–Altman (Fig. 3) plots. MRTM shows the poorest limits of agreement (i.e. 95% confidence interval equals 0.12, Fig. 3B) and the largest change in bias with binding (slope = 0.19 and $R^2=0.37$, Fig. 3B). All other methods showed better limits of agreement (≤0.08). Table 3 gives averages (±SD) of the differences plotted in Fig. 3 for three different ranges of BP^{SRTM}_{ND}. Reference tissue algorithms are known to perform worse at lower binding levels. Therefore the following analysis is restricted to higher levels of binding (BP^{SRTM}_{ND}>0.12, Table 3). Again, the noisiest results were obtained for MRTM (Table 3). Comparable performance was seen for all other methods in terms of linear regression (Fig. 2) and Bland–Altman (Fig. 3, Table 3) plots.

Parametric images

Fig. 4 shows typical parametric maps for an AD patient. In general, MRTMo, MRTM, MRTM3 and MRTM4 suffered from 'dot'-artefacts inside the brain due to extreme values. The number of these artefacts, i.e. outcomes with BP_{ND}>2 or BP_{ND}<−1, was highest for MRTM and consisted of 5.5% of the brain voxels. The number of these artefacts was less than 1.7% for MRTM, MRTMo, MRTM3 and MRTM4 and was 0% for reference Logan, RPM1 and RPM2. In addition, MRTM, reference Logan and RPM1 produced noisier BP_{ND} images than the other methods. Both RPM2 and MRTM2 showed low noise and no artefacts. Although MRTM2 and RPM2 provided similar contrast, RPM2 images showed somewhat higher BP_{ND} values than corresponding RPM1 and MRTM2 images.

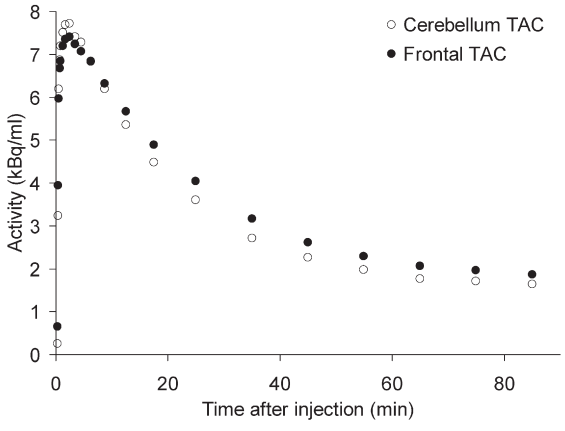

Fig. 1. Decay corrected TAC of [^{18}F]FDDNP in cerebellum and a frontal grey matter ROI. Data were taken from an AD subject.

Table 2
Linear regression parameters (slope, intercept and Pearson product moment correlation coefficient R^2) for several cortical regions in different subjects, including AD patients.

Parametric method	BP^{SRTM}_{ND}		
	R^2	Intercept	Slope
MRTMo	0.98 (0.02)	−0.02 (0.01)	1.07 (0.08)
MRTM	0.96 (0.04)	−0.01 (0.01)	1.18 (0.12)
MRTM2	0.98 (0.02)	0.01 (0.01)	1.03 (0.05)
MRTM3	0.98 (0.02)	−0.01 (0.01)	1.01 (0.06)
MRTM4	0.98 (0.02)	0.00 (0.01)	0.91 (0.05)
Reference Logan	0.98 (0.02)	0.01 (0.01)	0.88 (0.05)
RPM1	0.96 (0.08)	0.03 (0.01)	0.88 (0.10)
RPM2	0.98 (0.01)	0.00 (0.01)	1.11 (0.06)

BP_{ND} results from parametric methods were correlated against BP^{SRTM}_{ND}. Regression parameters were estimated for each subject. The table gives the averages (±SD) regression parameters.

Simulations

Without noise

First, different levels of binding for the target region were simulated. Accuracy of BP_{ND} obtained from each parametric method was evaluated relative to BP^{SRTM}_{ND}. In general, bias in parametric BP_{ND} was constant over the simulated range of binding levels (i.e. true BP_{ND} ranging from 0.03 to 0.48). Best BP_{ND} accuracy was achieved using both RPM methods (on average 0% bias, data not shown) and the highest bias was seen for reference Logan (on average −6% bias).

Next, changes in fractional blood volume were simulated. All parametric methods, except the two RPM methods, showed additional variation in accuracy due to changes in target V_b. All MRTM based algorithms showed the same behaviour, i.e. increasing V_b from 0.025 to 0.075 increased bias from 7 to 18% (data not shown). The largest variation in bias was seen for reference Logan, where for the same range in V_b, bias changed from 4 to −24% (data not shown). In contrast to variations in target V_b, variations in global V_b had no effect on the accuracy of any parametric method.

Finally, effects of changes in regional delivery on BP_{ND} accuracy were evaluated. These changes resulted in additional bias for all parametric methods (Table 4). Overall, the lowest bias was seen for RPM1, RPM2 and MRTM2. Changes in global delivery only affected accuracy of reference Logan. In this case, when K_1 decreased from 0.50 to 0.21, BP_{ND} bias increased from −2 to −39%.

Noise at voxel level

For these simulations the TAC noise level was set at 9% COV, which is comparable to noise at a voxel level seen in human studies. Again, accuracy of BP_{ND} was assessed by comparison with BP^{SRTM}_{ND}.

First, effects of different levels of binding were assessed. Table 5 summarizes bias in and precision of BP_{ND} for all parametric methods over the range of true BP_{ND} from (0.03 to 0.48. In general, compared with simulations without noise, for all parametric methods increased bias and poorer precision were seen, especially at lower levels of binding (Table 5). In addition, larger differences between methods were seen. The largest errors were seen for MRTM. Overall, best accuracy and precision were obtained for RPM2, followed by MRTM2, MRTM4 and reference Logan (Table 5).

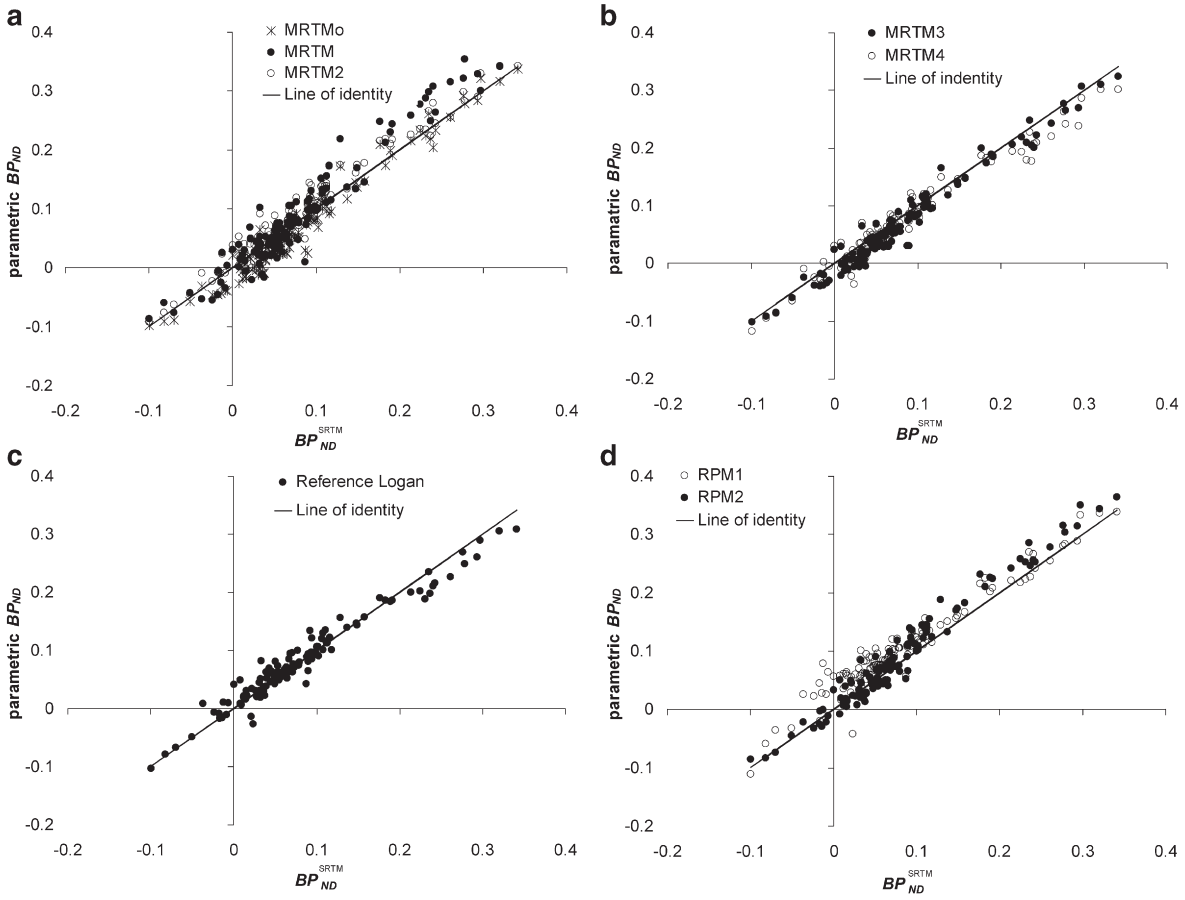

Fig. 2. Correlation of various parametric BP_{ND} with BP_{ND}^{SRTM} for human [^{18}F]FDDNP data, obtained from several subjects including AD patients.

Next, effects of variations in fractional blood volume were evaluated. Compared with simulations without noise no additional bias was observed for MRTM2, MRTM4, reference Logan and RPM2 (Table 6).

Finally, for all parametric methods, bias in BP_{ND} due to regional variations in delivery increased as a result of noise (Table 7). Similar to the simulations without noise, only reference Logan was affected by variations in global delivery. Overall, best accuracy of BP_{ND} was obtained for RPM2 and MRTM2.

Variable noise levels

Fig. 5 depicts accuracy and precision of several parametric methods as function of TAC noise level. Amongst all methods tested, RPM2 and MRTM2 showed best accuracy.

Discussion

In this study, the performance of various parametric methods for generating quantitative [^{18}F]FDDNP BP_{ND} images was evaluated, including methods in which the reference tissue efflux rate (k'_2) is fixed to a median value derived from all voxels. In a previous study it was shown that SRTM is the method of choice for analysing [^{18}F]FDDNP data. Indeed, SRTM provided more reproducible results than conventional plasma input models, even if labelled metabolites enter the brain (Yaqub et al., 2009). Therefore, SRTM was used as the standard with which all parametric methods were compared. Consequently, these parametric methods were all based on the use of a reference tissue. Performance was evaluated using both clinical and simulated data, focusing on BP_{ND}, as this is the parameter of interest. Simulated TAC data were generated using the standard reversible two tissue compartment plasma input model with kinetic parameters derived from clinical studies (Table 1). As mentioned above, however, all parametric methods were compared with SRTM applied to these TAC without adding noise.

Clinical assessment of parametric methods

BP_{ND} obtained with all parametric methods correlated strongly with BP_{ND}^{SRTM} (Fig. 2; R^2>0.9). These correlation graphs showed more bias at higher BP_{ND} levels for most methods. Closer analysis revealed a number of differences between the parametric methods evaluated. Firstly, MRTM produced noisier results than all other methods (Fig. 3B and Table 3). Secondly, qualitative assessment of parametric images showed that MRTMo, MRTM, MRTM3 and MRTM4 suffered from 'dot'-artefacts inside the brain due to outliers (Fig. 4). Thirdly, MRTM, reference Logan and RPM1 produced noisier BP_{ND} images than all other methods (Fig. 4). RPM1, MRTM and MRTMo do not make use of a fixed k'_2, a parameter that itself is sensitive to noise. As k'_2 should be the same for all tissue voxels, fixing it to an appropriate value should, at least in theory, result in more stable estimates (Wu and Carson 2002; Ichise et al., 2003). Finally, MRTM4 and reference Logan slightly underestimated BP_{ND} for higher levels of binding (Fig. 2). This may be due to noise, as several studies have shown that noise may result in additional parameter bias in linearized methods (Slifstein and Laruelle, 2000; Ichise et al., 2002). Note, however, that other parametric methods studied show some positive and/or negative bias as well.

Fig. 3. Bland–Altman plots of the human [^{18}F]FDDNP data. The differences are plotted versus the averages of parametric BP_{ND} and BP_{ND}^{SRTM}. Dashed lines show the limits of agreement (±2*SD from average). For each plot a linear regression line is given together with its equation and Pearson product moment correlation coefficient (R^2).

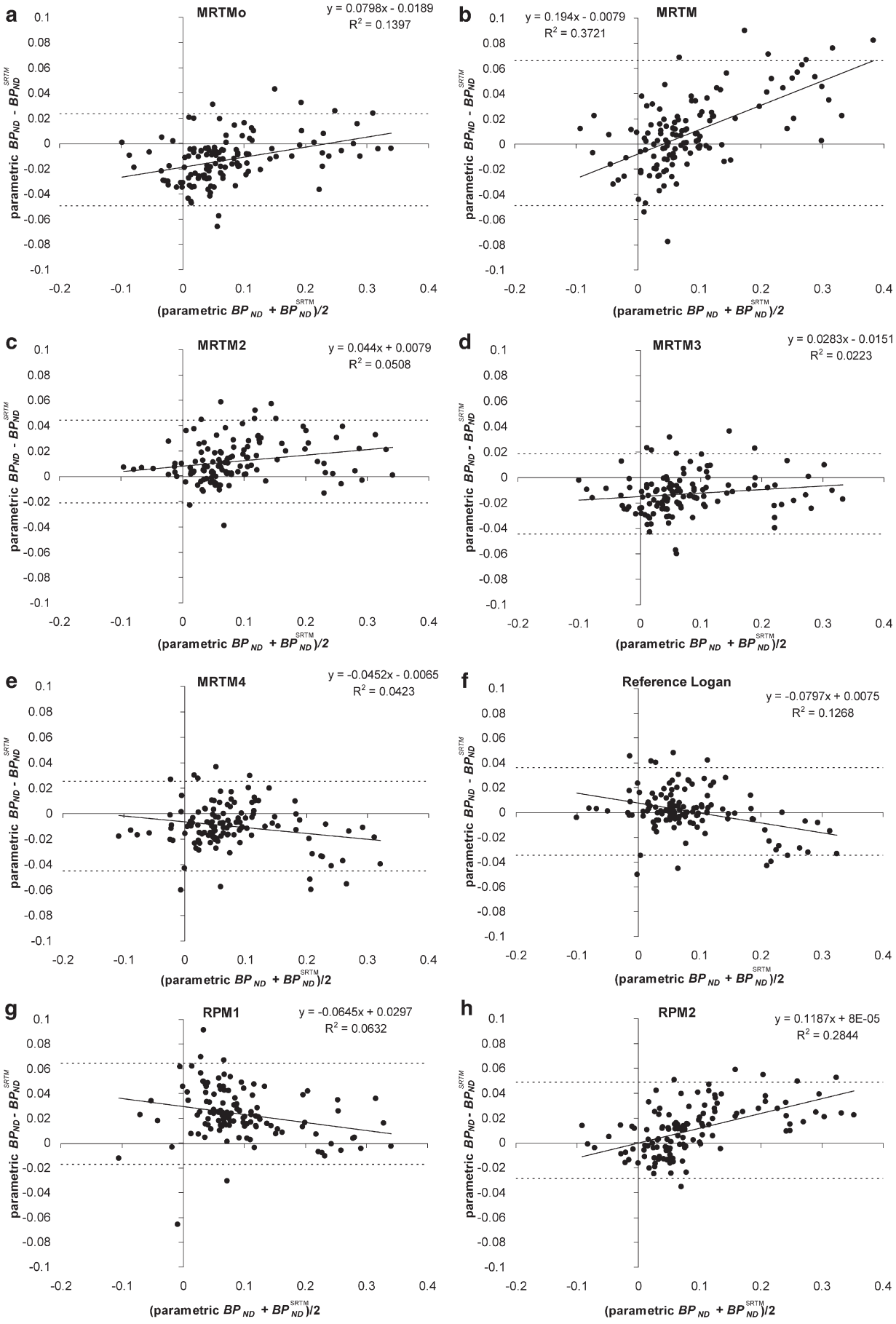
a
MRTMo
y = 0.0798x - 0.0189
R2 = 0.1397
b
MRTM
y = 0.194x - 0.0079
R2 = 0.3721
c
MRTM2
y = 0.044x + 0.0079
R2 = 0.0508
d
MRTM3
y = 0.0283x - 0.0151
R2 = 0.0223
e
MRTM4
y = -0.0452x - 0.0065
R2 = 0.0423
f
Reference Logan
y = -0.0797x + 0.0075
R2 = 0.1268
g
RPM1
y = -0.0645x + 0.0297
R2 = 0.0632
h
RPM2
y = 0.1187x + 8E-05
R2 = 0.2844
parametric BPND - BPNDSRTM
(parametric BPND + BPNDSRTM)/2

Table 3
Averages differences (±SD) derived from Bland–Altman plots (Fig. 3) for several intervals of BP_{ND}^{SRTM} values.

Parametric method	Average (±SD) of difference with BP_{ND}^{SRTM}		
	BP_{ND}^{SRTM} −0.2 to 0.12	BP_{ND}^{SRTM} 0.12 to 0.2	BP_{ND}^{SRTM} 0.2 to 0.4
MRTMo	−0.016 (0.017)	−0.003 (0.022)	−0.002 (0.016)
MRTM	0.002 (0.024)	0.031 (0.037)	0.045 (0.024)
MRTM2	0.011 (0.016)	0.025 (0.015)	0.011 (0.016)
MRTM3	−0.014 (0.015)	−0.001 (0.018)	−0.013 (0.015)
MRTM4	−0.008 (0.016)	−0.002 (0.011)	−0.032 (0.017)
Reference Logan	0.004 (0.016)	0.003 (0.011)	−0.024 (0.013)
RPM1	0.026 (0.020)	0.019 (0.013)	0.006 (0.016)
RPM2	0.006 (0.018)	0.031 (0.019)	0.026 (0.013)

Table 4
Bias of parametric BP_{ND} for TACs generated with several different target K_1 values.

Parametric method	K_1 (ml cm^{-3} min^{-1})				
	0.21	0.28	0.35	0.43	0.50
MRTMo	12%	5%	−1%	−3%	1%
MRTM	33%	9%	−1%	−3%	12%
MRTM2	2%	1%	−2%	−2%	−11%
MRTM3	12%	5%	−1%	−3%	1%
MRTM4	5%	2%	−1%	−3%	−12%
Reference Logan	−39%	−13%	−6%	−3%	−2%
RPM1	6%	−2%	0%	2%	0%
RPM2	6%	−2%	0%	2%	0%

Reference region K_1 was fixed to 0.35 ml·cm^{-3}·min^{-1}. TACs were simulated without noise. Bias is relative to BP_{ND}^{SRTM}.

In the present study, all parametric methods were compared with SRTM. As SRTM is based on non-linear regression, it is sensitive to noise, making it less suitable for calculations at the voxel level. Therefore, comparisons were performed at a ROI level. These comparisons could be compromised by heterogeneity within the ROI. To minimize the latter effects, ROI contained grey matter voxels only and were relatively small (5–20 cc). A disadvantage of comparing parametric images at a ROI level is that differences in noise levels between parametric images are reduced (smoothing effect). For example, differences in noise level in Table 3 (ROI level) are much smaller than those seen in the actual parametric images themselves (Fig. 4).

In summary, amongst all parametric methods evaluated, RPM2 and MRTM2 provided the best overall results for clinical data. These methods fix k'_2 to the median value estimated in an initial run, thereby effectively reducing noise induced bias and/or improving image quality, i.e. parametric maps produced by RPM2 and MRTM2, showed BP_{ND} images with good contrast, less noise and no 'dot'-artefacts.

Assessment of parametric methods using simulations

First, simulations were performed without noise in order to assess bias in the methods unrelated to noise. Overall best BP_{ND} accuracy was seen for RPM1 and RPM2, most likely because these algorithms are based on a basis function implementation of SRTM itself. There were no differences between RPM1 and RPM2 results. As expected, fixing k'_2 in case of noise free (perfect) data does not have an advantage. However, MRTM2, in which k'_2 is also fixed, performed better than MRTM. In the second run, MRTM2 has a fit term less than MRTM and therefore the overall fit equation is slightly different (Ichise et al., 2003).

The present simulations showed that each of the parametric methods is affected differently by regional variations in V_b and K_1. The largest bias was seen for reference Logan and overall best accuracy was observed for MRTM2, RPM1 and RPM2 (Table 4). Global changes in V_b and K_1 (i.e. similar changes in target and reference tissues) did not affect accuracy of the parametric methods, except for reference Logan.

More noise increased bias in BP_{ND} for all methods. Overall, poor accuracy and precision were seen for MRTM and best for RPM2 and MRTM2. Both RPM2 and MRTM2 performed better as a result of fixing k'_2, thereby reducing the number of fit parameters. Reference Logan also showed good performance. However, as mentioned above, this model was affected by variations in global K_1.

In summary, also in the simulations, best performance was seen for RPM2 and MRTM2.

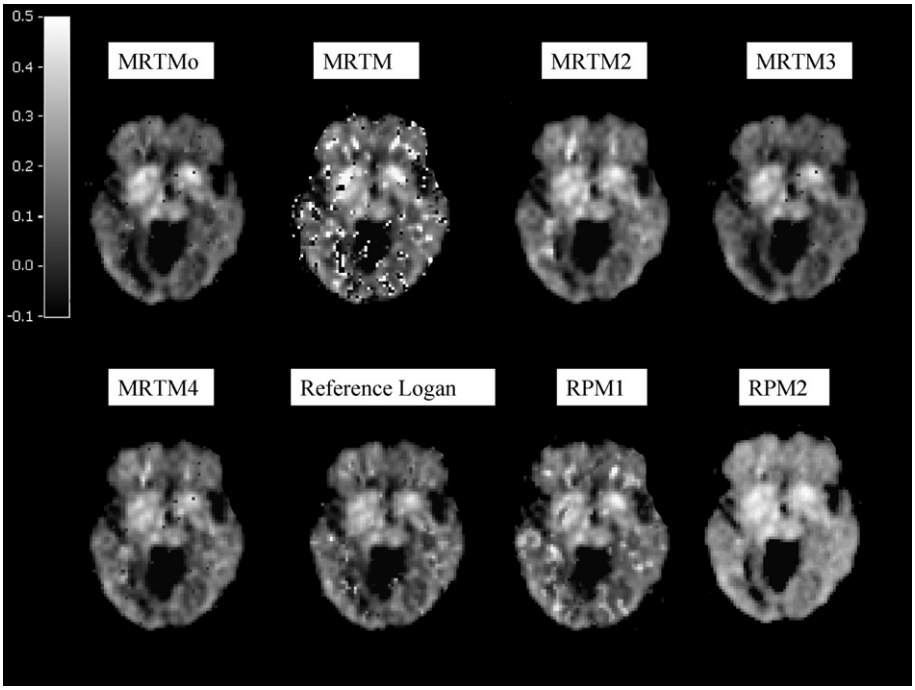

Fig. 4. Parametric [^{18}F]FDDNP BP_{ND} images for an axial plane through the middle of the brain in a typical AD subject. Eight different parametric methods were used. The same greyscale applies to all images and is restricted to the interval from −0.1 to 0.5.

Table 5
Bias of parametric BP_{ND} for TACs generated with different target BP_{ND} values, as given by BP_{ND}^{2T4ki}.

Parametric method	BP_{ND}^{2T4ki}				
	1.7	2	2.3	2.6	2.9
MRTMo	−16±98%	−15±19%	−14±13%	−14±9%	−13±9%
MRTM	−8±693%	−35±588%	4±116%	22±267%	−2±215%
MRTM2	28±153%	2±22%	−2±13%	−1±10%	0±8%
MRTM3	−17±98%	−12±18%	−13±12%	−13±8%	−12±7%
MRTM4	−50±167%	−3±24%	−5±13%	−3±11%	−1±8%
Reference Logan	−8±108%	−6±22%	−7±14%	−7±11%	−6±8%
RPM1	21±158%	18±40%	9±27%	5±20%	5±17%
RPM2	−9±98%	2±22%	0±14%	−2±10%	0±8%

TACs were simulated at 9% COV noise levels. Bias ± SD is relative to BP_{ND}^{SRTM}.

Table 7
Bias of parametric BP_{ND} for TACs generated with different target K_1 values.

Parametric method	K_1 (ml cm^{-3} min^{-1})				
	0.21	0.28	0.35	0.43	0.50
MRTMo	−83±48%	−34±26%	−15±19%	−6±18%	1±18%
MRTM	97±1187%	−10±456%	−35±588%	−1±100%	−1±301%
MRTM2	12±40%	2±26%	2±22%	1±24%	−9±25%
MRTM3	−63±33%	−30±23%	−12±18%	−6±17%	1±17%
MRTM4	1±43%	−3±28%	−3±24%	−11±26%	−20±28%
Reference Logan	−43±45%	−13±29%	−6±22%	−5±19%	−1±19%
RPM1	20±84%	19±53%	18±40%	−3±27%	−11±28%
RPM2	2±39%	2±27%	2±22%	−7±17%	−1±17%

Reference region K_1 was fixed to 0.35 ml cm^{-3} min^{-1}. TACs were simulated at 9% COV noise levels. Bias ± SD is relative to BP_{ND}^{SRTM}.

Conclusion

RPM2 and MRTM2 outperformed other parametric methods in both simulations and analysis of human data. These methods provided best accuracy and precision of estimated BP_{ND}, because of a reduction in number of fit parameters by estimating k'_2 in a first run and subsequently fixing to the median voxel value in the second. RPM2 and MRTM2 are therefore the methods of choice for parametric analysis of [^{18}F]FDDNP studies.

Acknowledgments

The authors would like to thank personnel of the Department of Nuclear Medicine & PET Research for tracer production and data acquisition. The authors would also like to thank the Netherlands Organisation for Scientific Research (VIDI grant 016.066.309), the American Health Assistance Foundation (grant A2005-026) and the Internationale Stichting Alzheimer Research (grant #05512) for financial support.

Appendix A. Overview of parametric algorithms

The parametric methods evaluated in the present study are all based on a reference tissue approach, thereby avoiding the need for arterial cannulation. The reference region consists of a single tissue compartment for the (free) tracer, with k'_1 and k'_2 giving influx (ml cm^{-3} min^{-1}) and efflux (min^{-1}) rate constants, respectively. These rate constants describe the exchange between plasma and reference region. In general, the target region consists of two tissue compartments, for free and bound tracer, respectively. K_1 (ml cm^{-3} min^{-1}), k_2 (min^{-1}), k_3 (min^{-1}) and k_4 (min^{-1}) are rate constants describing exchange between the various compartments for the target region. In case of methods based on the simplified reference tissue model (SRTM; Lammertsma and Hume, 1996) the target region consists of only one compartment containing both free and bound tracer. For SRTM, K_1 (ml cm^{-3} min^{-1}) and k_{2a} (min^{-1}) are rate constants, describing exchange between plasma and target tissue. Here k_{2a} equals $k_2/(1+k_3/k_4)$ in the two tissue compartment model mentioned above.

The reference tissue model is based on a number of assumptions. First, the contribution by fractional blood volume in tissue (V_b) is assumed to be negligible, which may be true after a certain time (t^*). In the present study the optimal t^* was estimated for each parametric method using several test runs and clinical data. This was required, as the same t^* is not necessarily optimal for all methods. In particular, a difference between reference Logan and the various MRTM methods was expected, as the first requires a fit to the (later) linear part of the plot only, whilst the latter are multi-linear approaches that allow for the inclusion of more data points. Next, influx and efflux ratios for reference and target tissues are assumed to be the same, i.e. $\frac{K'_1}{k'_2} = \frac{K_1}{k_2}$.

Table 6
Bias of parametric BP_{ND} for TACs generated with different target fractional blood volume (V_b) values.

Parametric method	V_b (%)		
	2.5	5	7.5
MRTMo	−4±21%	−15±19%	−33±17%
MRTM	−11±360%	−35±588%	−25±584
MRTM2	13±24%	2±22%	−15±20%
MRTM3	−1±21%	−12±18%	−30±17%
MRTM4	6±27%	−3±24%	−20±21%
Reference Logan	3±23%	−6±22%	−24±20%
RPM1	12±37%	18±40%	9±39%
RPM2	−1±21%	2±22%	−1±25%

Reference region V_b was fixed to 5%. TACs were simulated at 9% COV noise levels. Bias ± SD is relative to BP_{ND}^{SRTM}.

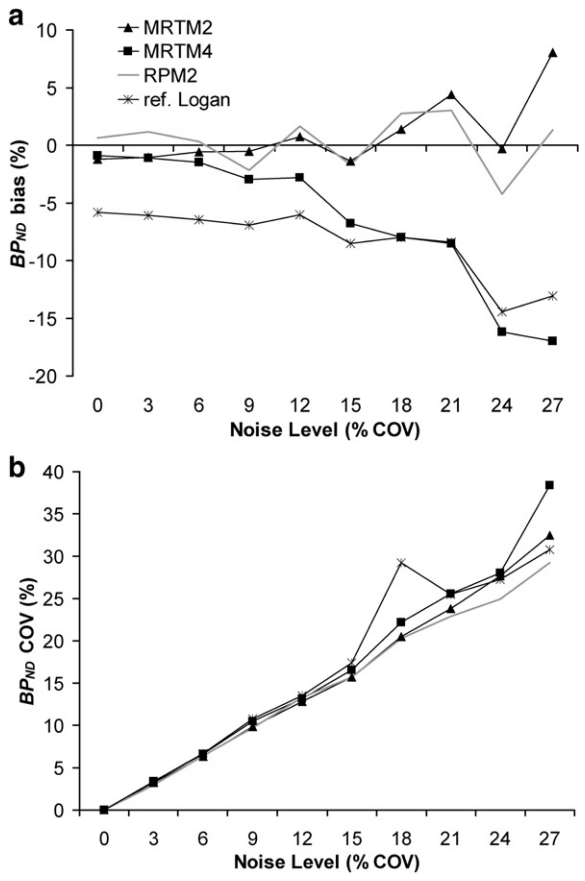

Fig. 5. Bias and COV of parametric BP_{ND} as function of (simulated) TAC noise level (% COV). Bias is relative to BP_{ND}^{SRTM}. COV reflects coefficient of variation of the bias.

Finally, it is assumed that $\frac{V_b C_P(t)}{C_{ND}(t)} \approx 0$ in the reference Logan method. Here, C_P is the concentration of the radioligand in plasma, and C_{ND} is the concentration of the radioligand in non-displaceable tissue, i.e. reference tissue.

Reference Logan

The reference Logan method (Logan et al., 1996) is based on solving the compartmental differential equations by integration and linearization, thereby reducing computation time and avoiding convergence problems as seen with non-linear methods. The equation for the reference Logan method is given by:

$$Y_1 = r_1 X_1 + term1 \quad (1)$$

with $Y_1 = \frac{\int_0^t C_T(t)dt}{C_T(t)}$, $X_1 = \frac{\int_0^t C_{ND}(t)dt}{C_T(t)}$, $r_1 = \frac{a}{a'}$, $term1 = -\frac{ab'}{a'}\frac{C_{ND}(t)}{C_T(t)} + b$, $b = -\frac{1}{k_2}$, $b' = -\frac{1}{k_2'}$, $a' = \frac{k_1'}{k_2'}$, $a = \frac{K_1}{k_2} + \frac{K_1 k_3}{k_2 k_4}$ and C_T is the concentration of radioligand in tissue.

Term 1 is constant, because in this model $\frac{C_T(t)}{C_{ND}(t)}$ is assumed to be constant, which may be true for certain tracers. For [^{18}F]FDDNP linear regression was performed using data beyond $t^* = 50$ min. The distribution volume ratio ($DVR = r_1$) and the binding potential ($BP_{ND} = r_1 - 1$) were then obtained from the resulting regression parameters.

MRTMo

The original Multi-linear Reference Tissue Method (MRTMo; Ichise et al., 2003) is based on the reference Logan method. However, in MRTMo, $\frac{C_T(t)}{C_{ND}(t)}$ is not assumed to be constant, and thus multi-linear regression is needed for analysis:

$$Y_1 = r_1 X_1 - r_2 X_2 + b \quad (2)$$

with $X_2 = \frac{C_{ND}(t)}{C_T(t)}$, and $r_2 = \frac{ab'}{a'}$. For [^{18}F]FDDNP, linear regression was performed using data beyond $t^* = 5$ min. R_1 ($= r_2 / b$), DVR ($= r_1$) and BP_{ND} ($= r_1 - 1$) were then estimated from the fit parameters.

MRTM

Rearrangement of Eq. (2) leads to MRTM (Ichise et al., 2003), which is given by the following equation:

$$Y_2 = \gamma_1 Z_1 + \gamma_2 Z_2 + \gamma_3 Z_3 \quad (3)$$

with $Y_2 = C_T(t)$, $Z_1 = \int_0^t C_{ND}(t)dt$, $Z_2 = \int_0^t C_T(t)dt$, $Z_3 = C_{ND}(t)$, $\gamma_1 = -\frac{a}{a'b}$, $\gamma_2 = \frac{1}{b}$ and $\gamma_3 = \frac{ab'}{a'b}$.. For [^{18}F]FDDNP, linear regression was performed using data beyond $t^* = 5$ min. After multi-linear regression BP_{ND} was estimated using $BP_{ND} = -\left(\frac{\gamma_1}{\gamma_2} + 1\right)$, k_2' using $k_2' = \frac{\gamma_1}{\gamma_3}$.

MRTM2

Rearrangement of MRTM leads to MRTM2 (Ichise et al., 2003):

$$Y_2 = \gamma_1 Z_4 + \gamma_2 Z_2 \quad (4)$$

with $Z_4 = \int_0^t C_{ND}(t)dt + b' C_{ND}(t)$, b' is fixed to the median $b'\left(= -\frac{1}{k_2'}\right)$ from all pixels with $BP_{ND} > 0$ taken from a first run using MRTM. For [^{18}F]FDDNP, linear regression was performed using data beyond $t^* = 5$ min. After multi-linear regression BP_{ND} was estimated using $BP_{ND} = -\left(\frac{\gamma_1}{\gamma_2} + 1\right)$ and, in case of a typical single tissue tracer, R_1 and k_2 using $R_1 = \frac{\gamma_1}{k_2'}$ and $k_2 = -\gamma_2$, respectively.

MRTM3

MRTM3 equals MRTMo with k_2' fixed to the median k_2' for all pixels with $BP_{ND} > 0$ from an initial run of MRTMo. For [^{18}F]FDDNP, linear regression was performed using data beyond $t^* = 5$ min.

MRTM4

MRTM4 equals MRTMo with k_2' fixed to the median k_2' for all pixels with $BP_{ND} > 0$ from an initial run of MRTM. For [^{18}F]FDDNP, linear regression was performed using data beyond $t^* = 5$ min.

RPM1

Reference parametric mapping (RPM1; Gunn et al., 1997) is an implementation of SRTM using basis functions in order to improve speed and avoid convergence problems. In this method, 40 basis functions were used. $\theta_3^{\min} = \frac{k_2^{\min}}{(1 + BP^{\max})}$ and $\theta_3^{\max} = k_2^{\max}$ were set to 0.01 and 0.3 min^{-1}, respectively (Gunn et al., 1997).

RPM2

RPM2 is preformed using RPM1 in two consecutive runs, as described by Wu and Carson (2002) for SRTM, in order to improve signal to noise ratio. In a first run of RPM1 the median k'_2 is estimated for all pixels with $BP_{ND} > 0$. Subsequently this is fixed to the median value in a second run. In this method, again 40 basis functions were used. $\theta_3^{\min} = \frac{k_2^{\min}}{(1 + BP^{\max})}$ and $\theta_3^{\max} = k_2^{\max}$ were set to 0.01 and 0.3 min^{-1}, respectively.

References

Adam, L.E., Zaers, J., Ostertag, H., Trojan, H., Bellemann, M.E., Brix, G., 1997. Performance evaluation of the whole-body PET scanner ECAT EXACT HR+ following the IEC standard. IEEE Trans. Nucl. Sci. 44, 1172–1179.

Barrio, J.R., Huang, S.C., Cole, G.M., Satyamurthy, N.M., Petric, A., Phelps, M.E., Small, G. W., 1999. PET imaging of tangles and plaques in Alzheimer disease. J. Nucl. Med. 40 (Suppl. S), 70–71.

Bland, J.M., Altman, D.G., 1986. Statistical-methods for assessing agreement between 2 methods of clinical measurement. Lancet 1, 307–310.

Braak, H., Braak, E., 1997. Frequency of stages of Alzheimer-related lesions in different age categories. Neurobiol. Aging 18, 351–357.

Brix, G., Zaers, J., Adam, L.E., Bellemann, M.E., Ostertag, H., Trojan, H., Haberkorn, U., Doll, J., Oberdorfer, F., Lorenz, W.J., 1997. Performance evaluation of a whole-body PET scanner using the NEMA protocol. J. Nucl. Med. 38, 1614–1623.

Defrise, M., Kinahan, P.E., Townsend, D.W., Michel, C., Sibomana, M., Newport, D.F., 1997. Exact and approximate rebinning algorithms for 3-D PET data. IEEE Trans. Med. Imaging 16, 145–158.

Gunn, R.N., Lammertsma, A.A., Hume, S.P., Cunningham, V.J., 1997. Parametric imaging of ligand-receptor binding in PET using a simplified reference region model. Neuroimage 6, 279–287.

Ichise, M., Toyama, H., Innis, R.B., Carson, R.E., 2002. Strategies to improve neuroreceptor parameter estimation by linear regression analysis. Journal of Cerebral Blood Flow and Metabolism 22, 1271–1281.

Ichise, M., Liow, J.S., Lu, J.Q., Takano, T., Model, K., Toyama, H., Suhara, T., Suzuki, T., Innis, R.B., Carson, T.E., 2003. Linearized reference tissue parametric imaging methods: application to [C-11]DASB positron emission tomography studies of the serotonin transporter in human brain. J. Cereb. Blood Flow Metab. 23, 1096–1112.

Joachim, C.L., Morris, J.H., Selkoe, D.J., 1989. Diffuse senile plaques occur commonly in the cerebellum in Alzheimer's disease. Am. J. Pathol. 135, 309–319.

Kepe, V., Shoghi-Jadid, K., Wu, H.M., Huang, S.C., Small, G.W., Satyamurthy, N., Petric, A., Phelps, M.E., Barrio, J.R., 2004. Global and regional [F-18]FDDNP binding as in vivo measure of Alzheimer's disease. J. Nucl. Med. 45 (Suppl.), 126.

Lammertsma, A.A., Hume, S.P., 1996. Simplified reference tissue model for PET receptor studies. Neuroimage 4, 153–158.

Logan, J., Fowler, J.S., Volkow, N.D., Wolf, A.P., Dewey, S.L., Schlyer, D.J., Macgregor, R.R., Hitzemann, R., Bendriem, B., Gatley, S.J., Christman, D.R., 1990. Graphical analysis of reversible radioligand binding from time activity measurements applied to [N-C-11-methyl]-(−)–cocaine pet studies in human-subjects. J. Cereb. Blood Flow Metab. 10, 740–747.

Logan, J., Fowler, J.S., Volkow, N.D., Wang, G.J., Ding, Y.S., Alexoff, D.L., 1996. Distribution volume ratios without blood sampling from graphical analysis of PET data. J. Cereb. Blood Flow Metab. 16, 834–840.

Lubberink, M., van Berckel, B.N.M., Luurtsema, G., Takkenkamp, K., Tolboom, N., Yaqub, M., Lammertsma, A.A., 2007. Multi-input spectral analysis for assessing cerebral uptake of labelled metabolites: validation and application to [11C]PIB and [18F] FDDNP studies. J. Cereb. Blood Flow Metab. 27 (BrainPET07 Abstract PS1-5M).

Luurtsema, G., Schuit, R.C., Takkenkamp, K., Lubberink, M., Hendrikse, N.H., Windhorst, A.D., Molthoff, C.F.M., Tolboom, N., van Berckel, B.N.M., Lammertsma, A.A., 2008. Peripheral metabolism of [18F]FDDNP and cerebral uptake of its labelled metabolites. Nucl. Med. Biol. 35 (8), 869–874.

Maes, F., Collignon, A., Vandermeulen, D., Marchal, G., Suetens, P., 1997. Multimodality image registration by maximization of mutual information. IEEE Trans. Med. Imaging 16, 187–198.

Petersen, R.C., Doody, R., Kurz, A., Mohs, R.C., Morris, J.C., Rabins, P.V., Ritchie, K., Rossor, M., Thal, L., Winblad, B., 2001. Current concepts in mild cognitive impairment. Arch. Neurol. 58, 1985–1992.

Shoghi-Jadid, K., Small, G.W., Agdeppa, E.D., Kepe, V., Ercoli, L.M., Siddarth, P., Read, S., Satyamurthy, N., Petric, A., Huang, S.C., Barrio, J.R., 2002. Localization of neurofibrillary tangles and beta-amyloid plaques in the brains of living patients with Alzheimer disease. Am. J. Geriatr. Psychiatry. 10, 24–35.

Slifstein, M., Laruelle, M., 2000. Effects of statistical noise on graphic analysis of PET neuroreceptor studies. Journal of Nuclear Medicine 41, 2083–2088.

Small, G.W., Kepe, V., Ercoli, L.M., Siddarth, P., Bookheimer, S.Y., Miller, K.J., Lavretsky, H., Burggren, A.C., Cole, G.M., Vinters, H.V., Thompson, P.M., Huang, S.C., Satyamurthy, N., Phelps, M.E., Barrio, J.R., 2006. PET of brain amyloid and tau in mild cognitive impairment. N. Engl. J. Med. 355, 2652–2663.

Smith, S.M., 2002. Fast robust automated brain extraction. Hum. Brain Map. 17, 143–155.

Svarer, C., Madsen, K., Hasselbalch, S.G., Pinborg, L.H., Haugbol, S., Frokjaer, V.G., Holm, S., Paulson, O.B., Knudsen, G.M., 2005. MR-based automatic delineation of volumes of interest in human brain PET images using probability maps. NeuroImage 24, 969–979.

Watson, C.C., 2000. New, faster, image-based scatter correction for 3D PET. IEEE Trans. Nucl. Sci. 47, 1587–1594.

West, J., Fitzpatrick, J.M., Wang, M.Y., Dawant, B.M., Maurer, C.R., Kessler, R.M., Maciunas, R.J., Barillot, C., Lemoine, D., Collignon, A., Maes, F., Suetens, P., Vandermeulen, D., vandenElsen, P.A., Napel, S., Sumanaweera, T.S., Harkness, B., Hemler, P.F., Hill, D.L.G., Hawkes, D.J., Studholme, C., Maintz, J.B.A., Viergever, M.A., Malandain, G., Pennec, X., Noz, M.E., Maguire, G.Q., Pollack, M., Pelizzari, C.A., Robb, R.A., Hanson, D., Woods, R.P., 1997. Comparison and evaluation of retrospective intermodality brain image registration techniques. J. Comput. Assist. Tomogr. 21, 554–566.

Wu, Y., Carson, R.E., 2002. Noise reduction in the simplified reference tissue model for neuroreceptor functional imaging. J. Cereb. Blood Flow Metab. 22, 1440–1452.

Yaqub, M., Boellaard, R., Kropholler, M.A., Lammertsma, A.A., 2006. Optimization algorithms and weighting factors for analysis of dynamic PET studies. Phys. Med. Biol. 51, 4217–4232.

Yaqub, M., Tolboom, N., Boellaard, R., van Berckel, B.N.M., van Tilburg, E.W., Luurtsema, G., Scheltens, P., Lammertsma, A.A., 2008. Simplified parametric methods for [C-11] PIB studies. NeuroImage 42, 76–86.

Yaqub, M., Boellaard, R., van Berckel, B.N.M., Tolboom, N., Luurtsema, G., Dijkstra, A.A., Lubberink, M., Windhorst, A.D., Scheltens, P., Lammertsma, A., 2009. Evaluation of tracer kinetic models for analysis of [18F]FDDNP studies. Mol. Imaging Biol. 11 (5), 322–333.

Zhou, Y., Resnick, S.M., Ye, W.G., Fan, H., Holt, D.P., Klunk, W.E., Mathis, C.A., Dannals, R., Wong, D.F., 2007. Using a reference tissue model with spatial constraint to quantify [C-11]Pittsburgh compound BPET for early diagnosis of Alzheimer's disease. NeuroImage 36, 298–312.